Investigational New Drugs (2019) 37:994–1005
https://doi.org/10.1007/s10637-018-00722-y

PRECLINICAL STUDIES

In vitro and in vivo cytotoxic activity and human serum albumin interaction for a methoxy-styryl-thiosemicarbazone

Otávio Augusto Chaves[1,2] · Isabela S. de Castro[3] · Carla Marins Goulart[2] · Myrtes S. S. Bellieny[2] · José Carlos Netto-Ferreira[2,4] · Juliana Echevarria-Lima[3] · Aurea Echevarria[2]

Received: 24 November 2018 / Accepted: 26 December 2018 / Published online: 19 January 2019

Summary

Thiosemicarbazone is a class of compounds with potential applications in medicine, presenting high capacity to inhibit the growth of cancer cells as well as low toxicity. Because of high interest in anticancer studies involving thiosemicarbazones as new chemotherapeutic agents, a synthetic thiosemicarbazone derivative, 4-*N*-(2′-methoxy-styryl)-thiosemicarbazone (MTSC) was evaluated *in vivo* against Ehrlich carcinoma in an animal model. *In vivo* results demonstrated that MTSC treatment induced the survival of mice and altered significantly the body weight of the surviving mice 12 days after tumor inoculation. Treatment with 30 mg/kg of MTSC exhibited effective cytotoxic activity with T/C values of 150.49% (1 dose) and 278% (2 doses). Its interaction with human serum albumin (HSA), which plays a crucial role in the biodistribution of a wide variety of ligands, was investigated by multiple spectroscopic techniques at 296 K, 303 K, and 310 K, as well as by theoretical calculations. The interaction between HSA and MTSC occurs *via* ground-state association in the subdomain IIA (Sudlow's site I). The binding is moderate ($K_a \approx 10^4\ M^{-1}$), spontaneous, entropically, and enthalpically driven. Molecular docking results suggested hydrogen bonding and hydrophobic interactions as the main binding forces. Overall, the interaction HSA:MTSC could provide therapeutic benefits, improving its cytotoxic efficacy and tolerability.

Keywords Thiosemicarbazones · Ehrlich carcinoma · Human serum albumin · Spectroscopy · Molecular docking

Introduction

Thiosemicarbazones belong to a class of compounds with potential applications in medicine because of their high ability to inhibit the growth of various pathogens and their low toxicity [1]. Among the biological activities, the thiosemicarbazone derivatives show potential application as antiviral [2], antimicrobial [3, 4], antiparasitic [5–7], and antitumor [8–10] agents. The anticancer effect of thiosemicarbazones is related to the inhibition of ribonucleotide reductase, an enzyme involved in the rate-limiting step of DNA synthesis [11]. Significant alterations in iron metabolism and iron-dependent enzymes of cancer cells contribute to the antitumor effect of thiosemicarbazones due to their iron-chelating properties [9, 12]. The antitumor activity of thiosemicarbazones has been evaluated *in vivo*, using lymphocytic leukemia—L1210, adenocarcinoma 755, Lewis lung carcinoma, and neuroblastoma, among others [13–15]. Ehrlich's ascites tumor is a very aggressive carcinoma characterized by a high level of cell proliferation and represents an important *in vivo* animal model [16].

Human serum albumin (HSA) is the most abundant carrier protein in the human circulatory system. It plays a crucial role in the transport, distribution, and metabolism of a wide variety of endogenous and exogenous ligands [17–19]. The crystallographic analysis of HSA revealed a monomeric globular protein structure composed of a single polypeptide chain

✉ José Carlos Netto-Ferreira
jcnetto.ufrrj@gmail.com

✉ Juliana Echevarria-Lima
juechevarria@micro.ufrj.br

1 Instituto SENAI de Inovação em Química Verde (ISI-QV), Rua Morais e Silva N° 53, Maracanã, Rio de Janeiro, RJ 20271-030, Brazil

2 Instituto de Química, Departamento de Química Orgânica, Universidade Federal Rural do Rio de Janeiro (UFRRJ), Rodovia BR-465, Km 7, Seropédica, RJ 23890-000, Brazil

3 Laboratório de Imunologia Básica e Aplicada, Depto. Imunologia, Instituto de Microbiologia Paulo de Góes, Universidade Federal do Rio de Janeiro (UFRJ), Av. Carlos Chagas Filho, 373, Rio de Janeiro, RJ 21941-590, Brazil

4 Qualidade e Tecnologia (INMETRO), Divisão de Metrologia Química, Instituto Nacional de Metrologia, Duque de Caxias, RJ 25250-020, Brazil

containing 585 amino acid residues (66 kDa), with three structurally similar domains (I, II, and III), each containing two subdomains (A and B) [20, 21]. As the therapeutic effect of a drug is directly related to its free concentration in plasma, it is of central pharmacological interest to study the drug–albumin binding ability [22, 23]. Several studies have dealt with the interaction between serum albumin and thiosemicarbazone derivatives [24–27]; however, no reports were found regarding 4-*N*-(2′-methoxy-styryl)-thiosemicarbazone (MTSC – Figure 1).

Because of our interest in anticancer/cytotoxic studies, as well as in thiosemicarbazones as novel chemotherapeutic agents, the synthetic derivative MTSC and its Cu(II) complex were assayed as *in vitro* cell viability as well as *in vivo* against Ehrlich carcinoma in an animal model using BALB/c mice. Because the efficacy of potential drugs is directly related to HSA binding ability, the present work also reports the study of interactions between HSA:MTSC using spectroscopic techniques (circular dichroism, steady-state, time-resolved, and synchronous fluorescence) combined with theoretical calculations (molecular docking). These data may contribute to a deeper understanding of the interaction mechanism, distribution, and transport involved in the association protein–thiosemicarbazone derivative, which is an important field of research in drug development.

Materials and Methods

Chemicals

2-methoxy-benzaldehyde and thiosemicarbazone, copper (II) chloride ($CuCl_2$), dimethyl sulfoxide (DMSO), 3-[4,5-dimethylthiazol-2-yl]-2,5-diphenyltetrazolium bromide (MTT), β-mercaptoethanol, *N*-(2-hydroxyethyl)piperazine-*N*′-(2-ethanesulfonic acid) (HEPES), penicillin, streptomycin, RPMI-1640 medium, human serum albumin (96-99% of purity), phosphate buffer solution (PBS), racemic ibuprofen and racemic warfarin were purchased from Sigma-Aldrich Chemical Company, St. Louis, USA, and used as received. One tablet of PBS yields 1.00×10^{-2} M phosphate buffer, 2.70×10^{-3} M potassium chloride and 1.37×10^{-1} M sodium chloride, pH 7.4, at 298 K. Fetal calf serum was obtained from Gibco, Life Technologies. Acetonitrile (spectrophotometric grade), methanol, ethanol, and sulfuric acid were obtained from Vetec Quimica Fina Ltda, RJ, Brazil.

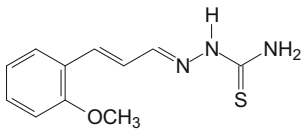

MTSC

Fig. 1 Chemical structure of 4-*N*-(2'-methoxy-styryl)-thiosemicarbazone (MTSC)

Synthesis

MTSC was synthesized and characterized as previously reported in the literature [5]. Briefly, an equimolar mixture of 2-methoxy-benzaldehyde and thiosemicarbazide was dissolved in ethanol in the presence of two drops of concentrated sulfuric acid and stirred by 1 h at 303 K. After removal of the solvent, the solid was recrystallized from methanol.

4-*N*-(2'-methoxy-styryl)-thiosemicarbazone (MTSC): Yield 82%; m. p. = 186-188°C; IR (ATR, cm^{-1}) ν 3420; 3383; 3240 (N-H); 3080 (C-H_{Ar}); 2970 (C-H_{alkyl}); 1594 (C=C); 1574; 1483; 1465 (C=C + C=N); 981 (C=C_{trans}); 823 (C=S_{free}). ^{1}H NMR (DMSO-d_6) δ (ppm) 11.34; 8.14; 7.87; 7.57; 7.31; 7.04; 6.98; 6.96; 3.85. ^{13}C NMR (DMSO-d_6) δ (ppm) 177.1; 156.4; 145.3; 133.5; 129.8; 127.0; 125.3; 120.3; 111.1; 55.0.

MTSC-complex was synthesized by the reaction between an equimolar mixture of MTSC and $CuCl_2$ dissolved in methanol:water (1:1, v/v) under reflux, for 1 h.

4-*N*-(2'-methoxy-styryl)-thiosemicarbazone-Cu(II)-complex (MTSC-complex): Yield 57%; m. p. = 207°C; IR (ATR, cm^{-1}) ν 3396 (N-H); 3070 (C-H_{Ar}); 2946 (C-H_{alkyl}); 1596 (C=C); 1548; 1485 (C=C + C=N); 980 (C=C_{trans}); 743 (C=$S_{complex}$). ^{1}H NMR (DMSO-d_6) δ (ppm) 11.35; 7,89; 7.62; 7.56; 7.32; 7.12; 7.05; 6.96; 6.91; 3.85. ^{13}C NMR (DMSO-d_6) δ (ppm) 178.1; 157.4; 146.0; 134.4; 130.7; 127.9; 126.3; 124.6; 121.3; 112.1; 56.0.

Biological assays

Animals

Inbred female BALB/c mice (2–4 months old) were used in all *in vivo* experiments. Animals were housed in a temperature-controlled room and received free access to water and standard rat chow (*ad libitum*). The experimental procedures were performed in accordance with the Brazilian Guidelines (Brazilian Directive for Care and Use of Animals for Teaching and Research-DBCA) published by the Brazilian Council for Control of Animal Experimentation (*Conselho Nacional de Controle de Experimentação Animal* – CONCEA) and Brazilian Federal Law 11.794 (October 8, 2008). Protocols used in this study were approved by the local research ethics committee of the *Universidade Federal Rural do Rio de Janeiro*, Brazil (Number 6985210617).

Cell culture

The human erythroleukemia K562, Lucena I (Vincristine-resistant derivative K562) and the Ehrlich ascites carcinoma

cell line were generously donated by Dr. Vivian M. Rumjanek from the *Instituto de Bioquímica Médica* of Universidade Federal do Rio de Janeiro (UFRJ). Burkett lymphoma Daudi cell lines were maintained in culture medium RPMI-1640, supplemented with β-mercaptoethanol (50 μmol/L), HEPES (25 mmol/L), penicillin (60 mg/L), streptomycin (100 mg/L), and 10% (v/v) fetal calf serum. Cells were incubated at 310 K in a humidified atmosphere of air and 5% CO_2. The cell lines were passaged twice a week at a density of 1.00×10^4 cells/mL.

Viability assay

Cells (1.00×10^4 cells/mL) were seeded on a 96-well cell culture plate and incubated in the presence or absence of either the MTSC or the MTSC–complex at a concentration of 3.12, 6.25, 12.50, 25.00, and 50.00 μM. The control groups comprised cells cultivated in the presence of either the vehicle (DMSO) or the medium. Cell viability was assessed by the addition of 20 μL/well of MTT (5 mg/mL) as described earlier [28]. This colorimetric assay is based on the conversion of the MTT (yellow) to the formazan (purple) derivative by mitochondrial enzymes in viable cells. The absorbance was measured on a microplate reader (Sunrise-Basic TECAN) at a wavelength of 490 nm.

In vivo evaluation of toxicity and cytotoxic activity

The toxicity was analyzed of treated BALB/c adult female mice with MTSC and MTSC–complex. Mice were treated with vehicle (DMSO; control group), 60 mg/kg of MTSC, or 60 mg/kg MTSC–complex once a week intraperitoneally (i.p.). After 30 days, the animals' weight, glucose level, and weight of heart, kidneys, liver, spleen, and thymus were analyzed. 2.50×10^5 of Ehrlich ascites carcinoma cells were injected i.p. in saline solution. After 24h mice were treated with vehicle (DMSO; control group 1), 30 mg/kg (group 2), or 60 mg/kg of MTSC (group 3) i.p. Seven days after tumor injection, groups 4 and 5 received a second injection (i.p.) of MTSC 30 mg/kg or 60 mg/kg, respectively. Thrice a week the weight of the mice was analyzed to correlate the tumor volume. After 70 days, the surviving mice were euthanized, and the weight of the body, heart, kidney, liver, spleen, and thymus was evaluated.

Statistical analysis

The values are given as mean ± SD. The IC_{50} value was calculated using the sigmoidaldose–response curve-fitting model using Prism 5 software. Evidence of drug effect is described by %T/C = [Δ tumor volume of a treated group]/[Δ tumor volume of control group] × 100%. Statistical analysis was performed by the Mann–Whitney U test. Values of $p \leq 0.05$ were considered statistically significant, using Prism 5 software.

HSA binding studies

Steady-state fluorescence experiments

The steady-state fluorescence measurements were performed on a Jasco model J-815 spectrofluorimeter equipped with a 1.0 cm quartz cell and a Jasco PFD-425S15F thermostat system with 0.1°C accuracy. All spectra were recorded with appropriate background corrections. The excitation wavelength of 280 nm was selected for the experiments and fluorescence spectra were obtained in the 290–450 nm range, at 296 K, 303 K, and 310 K. For the titration experiment, to a 3.0 mL solution containing HSA (1.00×10^{-5} M, in phosphate buffered saline (PBS) solution, pH 7.4), successive aliquots from an acetonitrile stock solution of MTSC (1.00×10^{-3} M) were added. The addition was performed manually with a 10 μL syringe, with varying concentrations of 0.17, 0.33, 0.50, 0.66, 0.83, 0.99, 1.15, and 1.32×10^{-5} M.

To compensate for the inner filter effect, the fluorescence intensity values of the samples containing HSA were corrected for the absorption of MTSC at excitation and emission wavelengths using Eq. (1) [29].

$$F_{cor} = F_{obs} 10^{[(A_{ex}+A_{em})/2]} \quad (1)$$

where F_{cor} and F_{obs} are the corrected and observed fluorescence intensity values, respectively, while A_{ex} and A_{em} represent absorbance values at the excitation (λ = 280 nm: ε = 13,998 $cm^{-1}M^{-1}$, in PBS) and emission wavelengths (λ = 340: ε = 41,762 $cm^{-1}M^{-1}$, in PBS), respectively.

The quenching of HSA fluorescence in the presence of increasing MTSC concentrations was analyzed using the Stern–Volmer equation—Eq. (2A)—and by the k_q definition—Eq. (2B) [30, 31]:

$$\frac{F_0}{F} = 1 + k_q \tau_0 [Q] = 1 + K_{SV}[Q] \quad (2A)$$

$$k_q = \frac{K_{SV}}{\tau_0} \quad (2B)$$

where F_0 and F represent the fluorescence intensity values of the HSA in the absence and presence of the MTSC, respectively, $[Q]$ is the ligand concentration. K_{SV} and k_q are the Stern–Volmer quenching constant and the bimolecular quenching rate constant, respectively. τ_0 is the lifetime of the fluorophore in the absence of ligand—the measured average value for the fluorescence lifetime of HSA was $(5.74 \pm 0.18) \times 10^{-9}$ s.

Data from the fluorescence quenching experiments were used to calculate the modified Stern–Volmer binding constant (K_a) of HSA with MTSC according to the method of the modified Stern–Volmer equation–Eq. (3) [32, 33]:

$$\frac{F_0}{F_0 - F} = \frac{1}{f[Q]K_a} + \frac{1}{f} \quad (3)$$

where F_0 and F are the steady-state fluorescence intensities in the absence and presence of MTSC, respectively; f is the fraction of the initial fluorescence intensity corresponding to a fluorophore that is accessible to the quencher ($f \approx 1.00$) and [Q] the MTSC concentration.

The thermodynamic parameters ($\Delta H°$, enthalpy change, and $\Delta S°$, entropy change) for the HSA:MTSC interaction were obtained from the van't Hoff plot using Eq. (4A) and the Gibbs free energy change values ($\Delta G°$) were obtained from Eq. (4B) [34, 35]:

$$\ln K_a = -\frac{\Delta H^0}{RT} + \frac{\Delta S^0}{R} \quad (4A)$$

$$\Delta G^0 = \Delta H^0 - T\Delta S^0 \quad (4B)$$

where T is the temperature (296 K, 303 K, and 310 K) and R is the gas constant (8.3145 $Jmol^{-1}K^{-1}$).

Time-resolved fluorescence experiments

Time-resolved fluorescence measurements were performed on spectrofluorimeter model FL920 CD from Edinburgh Instruments equipped with an EPL laser (λ_{exc} = 280 ± 10 nm; a pulse of 850 ps with an energy of 1.8 μW/pulse, monitoring emission at 340 nm). Fluorescence decay for the free HSA solution (1.00×10^{-5} M in PBS, pH = 7.4) and for an HSA solution containing the maximum concentration of MTSC used in the steady-state fluorescence studies (1.32×10^{-5} M) was obtained at room temperature (*ca* 298 K).

Synchronous fluorescence experiments

Synchronous fluorescence (SF) experiments were performed in an Edinburgh Instruments fluorimeter model Xe900. SF spectra for HSA (1.00×10^{-5} M) were recorded with increasing concentration of MTSC (0.17, 0.33, 0.50, 0.66, 0.83, 0.99, 1.15, and 1.32×10^{-5} M) by setting $\Delta\lambda$ = 60 nm and $\Delta\lambda$ = 15 nm for tryptophan and tyrosine residues, respectively, in the 240–320 nm range, at room temperature (*ca* 298 K).

Circular dichroism spectra measurements

CD spectra were obtained using a Jasco J-815 spectropolarimeter equipped with a Jasco PFD-425S15F thermostated system with 0.1°C accuracy. HSA concentration was kept constant at 1.00×10^{-6} M and the ligand concentration was set as the maximum concentration used in the steady-state fluorescence studies (1.32×10^{-5} M). CD spectra were measured in the 200–260 nm range, at 310 K. All spectra were recorded with appropriate background corrections.

The intensity of the CD signal was expressed as mean residue ellipticity (MRE), defined according to Eq. (5) [35]:

$$MRE = \frac{\theta}{(10.n.l.C_P)} \quad (5)$$

where θ is the observed CD (in millidegree), n is the number of amino acid residues (585 for HSA) [36], l is the path length of the cell (in cm), and C_p is the molar concentration of HSA (1.00×10^{-6} M). The α-helical contents of free HSA and bound to MTSC were calculated from the MRE values at 208—Eq. (6A)—and 222 nm—Eq. (6B) [31, 37]:

$$\alpha\text{-}helix\% = \left[\frac{(-MRE_{208} - 4000)}{(33000 - 4000)}\right] \times 100 \quad (6A)$$

$$\alpha\text{-}helix\% = \frac{(-MRE_{222} - 2340)}{30300} \times 100 \quad (6B)$$

Competitive binding studies

Competitive binding studies were carried out using the site probes for Sites I and II, *e.g.*, warfarin and ibuprofen, respectively. HSA and site probes were used at a fixed concentration (1.00×10^{-5} M), and the fluorescence quenching titration with MTSC was performed as described previously for the steady-state fluorescence quenching procedure, at 310 K. For each data point, the inner filter correction was made as shown in Eq. (1) and the K_a value in the presence of each site marker was obtained from Eq. (3).

Molecular docking

The crystallographic structure of HSA was obtained from the Protein Data Bank (PDB) with access code 1N5U [20]. The MTSC structure was built and energy-minimized by Density Functional Theory (DFT) calculations (B3LYP potential) with basis set 6-31G*, available in the Spartan'14 program (Wavefunction, Inc.).

The molecular docking studies were performed with the GOLD 5.2 program (CCDC, Cambridge Crystallographic Data Centre). Hydrogen atoms were added to the protein according to the data inferred by the program on the ionization and tautomeric states. The docking interaction cavity in the protein was established with a 10 Å radius from the Trp-214 residue (this amino acid residue was chosen for docking exploration based on the steady-state fluorescence and competitive binding studies described in the "Results and Discussion" section) [21]. The number of genetic operations (crossover, migration, mutation) in each docking run used in the search procedure was set to 100,000. The program optimizes hydrogen-bond geometries by rotating the hydroxyl and the amino groups present on the amino acid. The scoring

function used was "*ChemPLP*," which is the default function of the GOLD 5.2 program. The score of each pose identified was calculated as the negative of the sum of a series of energy terms involved in the protein–ligand interaction process, so that the more positive the score, the better is the interaction. The graphical representations of the best scores were generated with the PyMOL program (DeLano Scientific LLC).

Results and Discussion

Evaluation of cytotoxic activity

Effect on cell viability in vitro

To investigate the ability of MTSC and its Cu(II) complex to induce cell death *in vitro*, the human K562 erythroleukemia cell lines and Lucena I (Vincristine-resistant derivative K562) were used. Cells were incubated with different concentrations of either MTSC or MTSC–complex for 72h. Using the MTT assay, it was observed that MTSC induced cell death in K562 cells (IC_{50}= 20.5 ± 1.8 μM) and Lucena I (IC_{50}= 12.8 ± 1.0 μM). Similar results were observed with MTSC–complex treating Lucena I cells (IC_{50}= 9.1 ± 0.2 μM). In other studies, thiosemicarbazone derivatives have been shown to have antiproliferative activity and to induce cell cycle arrest in the G2/M phase in tumor cells [38, 39]. In addition, the cytotoxic activity of thiosemicarbazone derivatives can also be related to the inhibition of topoisomerase IIα [40, 41]. Although we have not studied the mechanism of action of MTSC, these already described routes can be responsible for the results observed by us.

Analysis of toxicity of MTSC and MTSC–complex in vivo

Adult BALB/c female mice were treated with 20 mg/kg of MTSC or MTSC–complex once a week. After 30 days, the weight of the animal, glucose levels, and the weight of the heart, kidneys, liver, spleen, and thymus were analyzed (Table 1).

Table 1 *In vivo* parameters for the vehicle, MTSC, and MTSC–complex—the compounds did not induce toxicity *in vivo*

Parameter	Vehicle[a]	MTSC[a]	MTSC–complex[a]
Body weight	22.000 ± 0.700	22.000 ± 0.700	21.500 ± 0.700
Heart weight	0.111 ± 0.003	0.116 ± 0.005	0.111 ± 0.006
Kidney weight	0.164 ± 0.007	0.172 ± 0.012	0.157 ± 0.003
Liver weight	1.108 ± 0.050	1.161 ± 0.070	0.972 ± 0.050
Spleen weight	0.101 ± 0.005	0.110 ± 0.003	0.109 ± 0.005
Thymus weight	0.500 ± 0.005	0.560 ± 0.001	0.560 ± 0.003

a. The values are expressed as Mean ± Standard Error

Our results demonstrated that treatment of mice with MTSC or with MTSC–complex did not alter the weight of heart, kidneys, liver, or the body weight. In addition, analysis of the subpopulations of $CD4^+$ and $CD8^+$ T lymphocytes from lymph nodes and spleen did not result in any difference (data not shown). However, treatment with MTSC–complex induced a dangerous increase in glucose levels (345.0 ± 141.8 mg/dL) when compared with the vehicle (DMSO) or MTSC (117 ± 19.97 and 98.67 ± 3.18 mg/dL, respectively). Therefore, only the *in vivo* cytotoxic activity of MTSC was investigated.

In vivo cytotoxic activity of MTSC

To evaluate the cytotoxic activity of MTSC *in vivo*, two strategies were used: 1) mice were treated with an injection (i.p.) of MTSC 24 h after tumor inoculation; 2) mice were treated with two injections with half the dose of MTSC (i.p.) 24 h and 6 days after tumor inoculation.

Our results demonstrated that treatment with 30 mg/mL of MTSC using both strategies significantly altered the body weight of surviving mice 12 days after tumor inoculation (Figures 2a and b). The mean weight of the Ehrlich tumor-inoculated and vehicle-treated mice was 29.08 g. On the other hand, after treatment with a dose of 30 mg/mL of MTSC the body weight of the mice was 24.92 g, whereas after treatment with two doses of 30 mg/mL each of MTSC was 25.70 g. In Figures 2c and d, it can be seen that the treatment with MTSC induced the survival of the mice. Evidence of compound effect is described by the equation %T/C = [increase in the survival time of treated mice (T)]/[increase in the survival time of vehicle group (C)] × 100. In Table 2, it can be observed that 30 mg/kg of MTSC exhibited effective cytotoxic activity with T/C values of 150.49% (1 dose) and 278% (2 doses). These values for %T/C indicate a significant cytotoxic activity. Furthermore, after 70 days, the surviving mice did not exhibit ascites. The mice were then euthanized and the analysis of both body weight and heart, kidney, liver, spleen, and thymus was similar to that observed in healthy mice (without tumor). The *in vivo* effect of other thiosemicarbazone derivatives on the development of Ehrlich solid tumor in mice has been extensively investigated. As an example, 30 mg/kg of thiophene-thiosemicarbazone derivatives inhibited tumor growth by approximately 71% [39]. Interestingly, some phase I clinical trials using thiosemicarbazones have now been performed, confirming the promising cytotoxic activity of this class of compound.

Binding characterization between HSA:MTSC

Some drugs are able to bind to albumin and this interaction determines tissue drug delivery [42]. Matsumura and Maeda [43] demonstrated that albumin accumulated within the interstitium of solid tumors, promoting a retention effect. Steady-state fluorescence quenching is a sensitive technique for

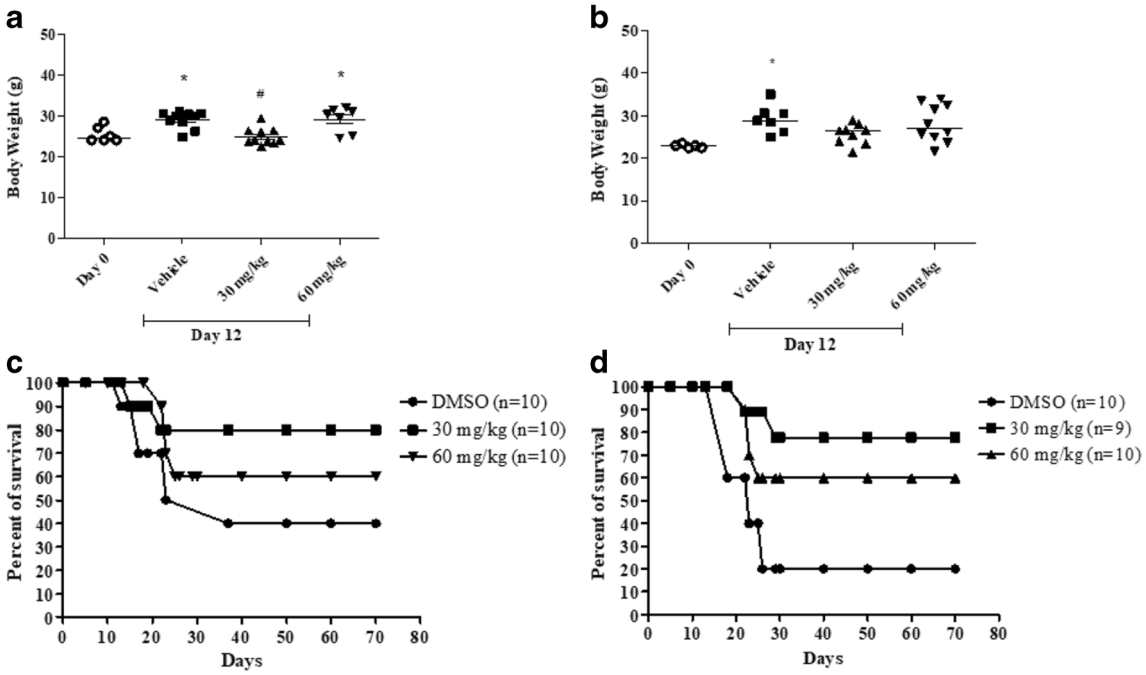

Fig. 2 Cytotoxic activity of MTSC. 2.50×10^5 of Ehrlich ascites carcinoma cells were injected (i.p.). Mice were treated with one dose (i.p.) of MTSC (30 or 60 mg/mL) or vehicle (**a** and **b**) 24h after tumor inoculation; Mice were treated with two doses (**c** and **d**). 24h after tumor inoculation mice were treated with vehicle or 15 or 30 mg/mL of MTSC, and then 6 days animals received the same treatment (15 or 30 mg/mL of MTSC or vehicle). The efficiency of the ascitic tumor treatment was determined by the increase in the survival time of the treated mice as compared with that of the vehicle group. $^{\#,*}p < 0.05$

monitoring drug binding to serum albumin due to its accuracy, rapidity, and ease of use at low concentrations under physiological conditions [44]. Figure 3a shows HSA fluorescence quenching by successive additions of the potential drug MTSC, at 310 K. This quenching process indicates that MTSC is located next to the intrinsic albumin fluorophore, *i.e.*, the Trp-214 residue. Furthermore, the emission maxima and shape of the peaks changed with increasing concentration of MTSC (blue shift, from 340 (HSA) to 331 nm (HSA:MTSC), indicating that MTSC may exert some influence on the polarity of the microenvironment inside the cavity where the Trp-214 residue can be found [45].

To obtain a deeper understanding of the fluorescence quenching mechanism—if static and/or dynamic—the steady-state fluorescence data were analyzed using both the Stern–Volmer equation and the k_q definition—Eqs. (2A) and (2B) [46]. As listed in Table 3, the Stern–Volmer quenching constant values (K_{SV}) decrease with increasing temperature and the bimolecular quenching rate constant values (k_q) are higher than the limiting diffusion rate constant in water ($k_{diff} \approx 7.40 \times 10^9$ $M^{-1}s^{-1}$, according to Smoluchowski–Stokes–Einstein theory at 298 K) [47]. This is a clear indication that the main fluorescence quenching takes place *via* a static process. This static mechanism probably originates from a ground-state association between Trp-214 and the potential drug MTSC [48].

Table 2 *In vivo* effects of MTSC against Ehrlich tumor

Treatment	Days after tumor inoculation	Dose (mg/kg)	%T/C
Vehicle	1	–	100
Vehicle	1and 6	–	100
MTSC 1 dose	1	30	150.49
MTSC 1 dose	1	60	73.89
MTSC 2 doses	1and 6	15 and 15	278
MTSC 2 doses	1and 6	30 and 30	253.5

a. %T/C ≥ 125 for significant cytotoxic activity

To confirm further the fluorescence quenching mechanism involved in the association HSA:MTSC, time-resolved fluorescence spectroscopy measurements were carried out and the decay profile obtained is depicted in Figure 3b. Fluorescence lifetimes for free HSA and for HSA:MTSC, (MTSC at the maximum concentration used in the steady-state fluorescence studies) did not vary significantly, ranging from $\tau_1 = 1.46 \pm 0.16$ (19.0%), $\tau_2 = 5.74 \pm 0.18$ (81.0%) ($\chi^2 = 1.158$, for HSA) to $\tau_1 = 1.43 \pm 0.15$ (18.5%), $\tau_2 = 5.70 \pm 0.17$ (81.5%) ($\chi^2 = 1.171$, for HSA:MTSC). From these results, it can be seen that the fluorescence lifetime of free HSA is unaffected by the presence of the potential drug, which is an indication that the fluorescence quenching mechanism is static, and implies a ground-state association between the tryptophan residue in HSA and MTSC [27, 49].

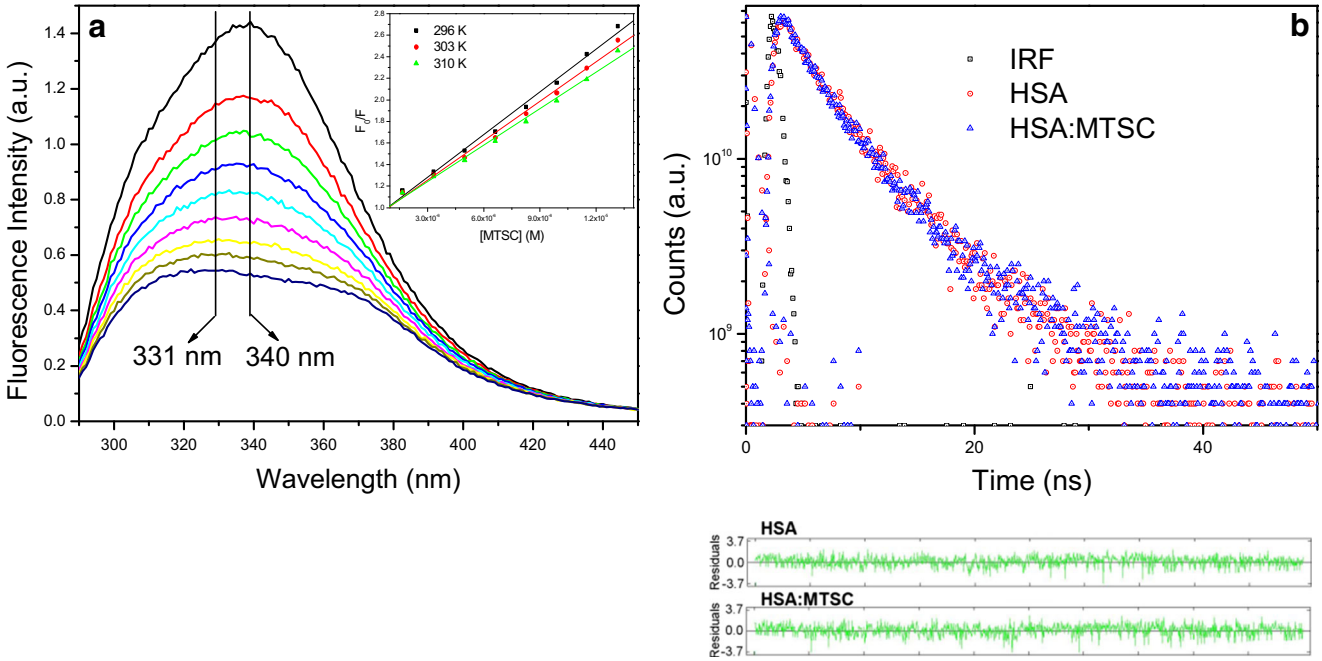

Fig. 3 **a** Steady-state fluorescence emission spectra for free HSA and its quenching by MTSC in PBS (pH = 7.4) at 310 K. Inset: Stern–Volmer plots for the interaction HSA:MTSC at 296 K, 303 K, and 310 K. **b** Time-resolved fluorescence decays and its residuals for HSA solution and HSA:MTSC at room temperature. [HSA] = 1.00×10^{-5} M, [MTSC] = 0.17, 0.33, 0.50, 0.66, 0.83, 0.99, 1.15, and 1.32×10^{-5} M

The evaluation of the modified Stern–Volmer binding constant (K_a) between serum albumin and a ligand is important to understand its distribution in plasma and organs. A too-weak binding can lead to a poor distribution of the molecule in the body, while strong binding decreases the concentration of free molecules in plasma. Therefore, moderate binding constant values can be set as the best parameter to achieve the desired biological activity for many potential drugs [50]. Table 3 lists the obtained $K_a$values for HSA:MTSC, with the corresponding modified Stern–Volmer plots being presented in Figure 4. The K_a values are in the order of 10^4 M^{-1}, indicating a moderate interaction between human serum albumin and MTSC [25, 26, 45]. Clearly, the decreasing trend of K_a values with temperature increase is consistent with the K_{SV} dependence on temperature, being in total agreement with the static fluorescence quenching mechanism already discussed [48].

The main noncovalent forces promoting interactions between ligands and proteins can be attributed to hydrogen bonds, van der Waals forces, hydrophobic, and electrostatic interactions [51].

Thermodynamic parameters, including enthalpy change ($\Delta H°$), entropy change ($\Delta S°$), and Gibbs free energy change ($\Delta G°$) confirm the driving forces of the binding [48]. To elucidate the interaction of HSA with MTSC, the thermodynamic parameters $\Delta H°$ and $\Delta S°$ were calculated from the van't Hoff plot (inset in Figure 4). The negative enthalpy change ($\Delta H°$) and positive entropy change ($\Delta S°$) values (Table 3) are a consequence of the dominant influence of hydrogen bonding and hydrophobic forces in the interaction process [52]. Consequently, the negative Gibbs free energy change values ($\Delta G°$, Table 3) characterize the binding as a spontaneous process. From the thermodynamic analysis, binding between HSA:MTSC is entropically and enthalpically driven because both enthalpy and entropy change values contribute to the spontaneity of the binding process [18]. The obtained results are in agreement with those reported in the literature for benzaldehyde thiosemicarbazone and some of its fluorinated derivatives [25, 27].

According to Miller's theory, when the interval between the excitation and emission wavelengths ($\Delta\lambda$) is set at

Table 3 Stern–Volmer quenching constant (K_{SV}), bimolecular quenching rate constant (k_q), modified Stern-Volmer binding constant (K_a), and thermodynamic parameters ($\Delta H°$, $\Delta S°$ and $\Delta G°$) for the interaction HSA:MTSC at 296 K, 303 K, and 310 K

T (K)	K_{SV} ($\times 10^5$) (M^{-1})	k_q ($\times 10^{13}$) ($M^{-1}s^{-1}$)	r^2	K_a ($\times 10^4$) (M^{-1})	r^2	$\Delta H°$ (kJmol^{-1})	$\Delta S°$ (kJmol^{-1}K^{-1})	$\Delta G°$ (kJmol^{-1})	r^2
296	1.32 ± 0.05	2.30	0.9967	7.11 ± 0.26	0.9999	11.6 ± 1.1	0.0537 ± 0.0021	–27.5	0.9997
303	1.22 ± 0.04	2.13	0.9967	6.40 ± 0.26	0.9999			–27.9	
310	1.13 ± 0.04	1.97	0.9962	5.75 ± 0.26	0.9998			–28.2	

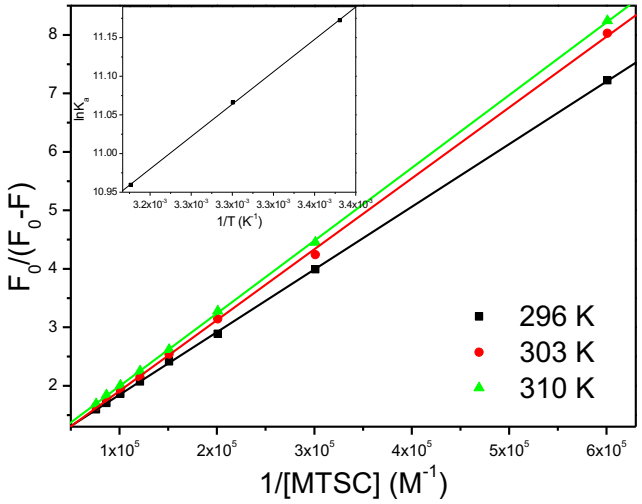

Fig. 4 Modified Stern-Volmer plots for the interaction between HSA:MTSC (pH = 7.4) at 296 K, 303 K, and 310 K. Inset: van´t Hoff plot for HSA:MTSC

15 nm or 60 nm, the synchronous fluorescence spectra (SFS) of serum albumin can offer characteristic information about the Tyr or Trp residues, respectively [53]. In other words, SFS can provide information about the molecular environment in the vicinity of internal chromophores of a protein, by scanning the excitation and emission monochromators simultaneously, while maintaining a constant wavelength interval (Δλ) between them [54]. As can be seen in Figure 5a, the maximum fluorescence emission wavelength for the Tyr residue shows no significant shift after successive additions of MTSC, indicating that the microenvironment around the Tyr residue was not altered by the presence of MTSC [31]. For the Trp residue, a clear blue shift in the synchronous fluorescence spectrum can be observed after successive additions of MTSC (Figure 5b). This behavior probably expresses an increase in the hydrophobicity surrounding the Trp residue [51]. These results clearly confirm the data obtained from the steady-state fluorescence quenching, *i.e.*, that the binding could affect the polarity around the tryptophan residue.

Circular dichroism (CD) is an excellent tool for rapid determination of the secondary structure of proteins. As depicted in Figure 6, the CD spectrum of HSA shows two negative signals: one at 208 nm and other at 222 nm, characteristic of $\pi \rightarrow \pi^*$ and $n \rightarrow \pi^*$ transitions of carbonyl groups in a polypeptide chain, respectively [54]. After the addition of MTSC, the CD spectrum of HSA shows a gradual loss in intensity at 222 and 208 nm (becomes less negative), which indicates the loss of α-helix content [55]. The quantitative estimation of α-helix content suggests a weak perturbation on the secondary structures of HSA after the addition of MTSC, from 63.3% to 61.8%, at 208 nm and from 58.3% to 56.9%, at 222 nm. It has been reported that some fluorinated derivatives of thiosemicarbazone benzaldehyde also do not significantly alter the secondary structure of HSA [27].

As previously described by Sudlow *et al.*, there are two main binding sites in human plasma albumin for different classes of drugs: one is located in subdomain IIA, namely Sudlow's site I (warfarin binding site) and the other is located in subdomain IIIA, namely Sudlow's site II (ibuprofen binding site) [56]. To identify the main binding sites for MTSC on HSA, site marker competitive experiments were carried out. The modified Stern–Volmer binding constant (K_a) was calculated in the presence of each site probe (warfarin and ibuprofen), at 310 K and the plots are shown in Figure 7. In the presence of warfarin, K_a values were significantly changed (60.9%, from 5.75×10^4 to 2.25×10^4 M^{-1}) while the influence of ibuprofen in the binding parameter was not significant (7.83%, from 5.75×10^4 to 5.30×10^4 M^{-1}). These results indicate a competition between warfarin and the potential drug for the same binding site in HSA [54]. Therefore, MTSC binds in Sudlow's site I (subdomain IIA) of HSA, where the Trp-214

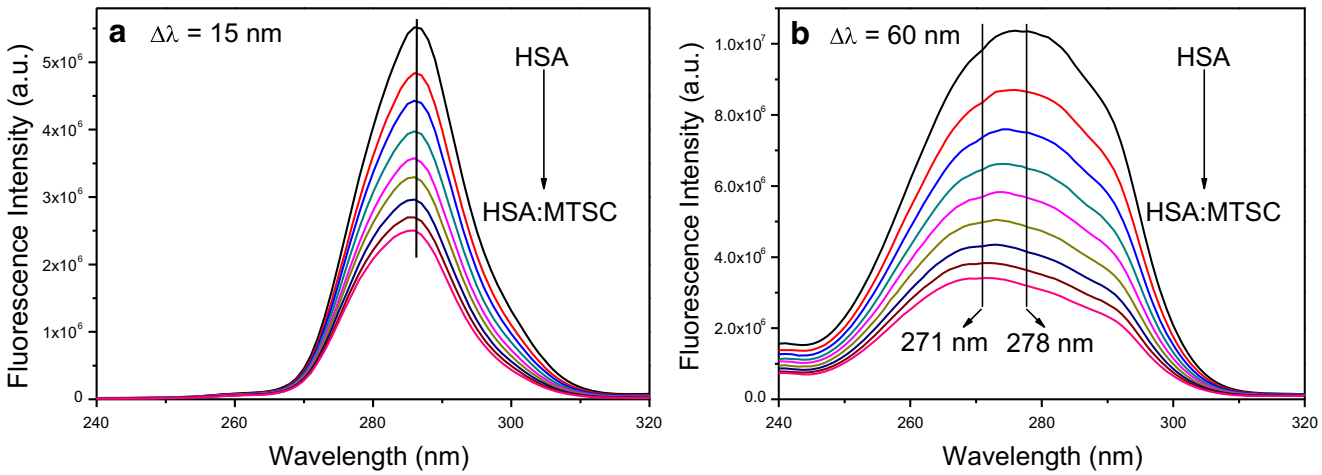

Fig. 5 Synchronous fluorescence measurement for HSA without and with the presence of MTSC with Δλ = 15 nm for Tyr (**a**) and Δλ = 60 nm for Trp (**b**). [HSA] = 1.00×10^{-5} M, [MTSC] = 0.17, 0.33, 0.50, 0.66, 0.83, 0.99, 1.15, and 1.32×10^{-5} M and pH = 7.4 at room temperature

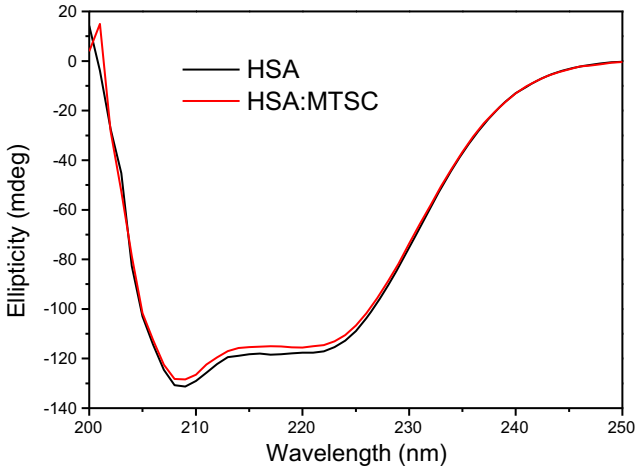

Fig. 6 Circular dichroism spectra for free HSA and HSA:MTSC, pH = 7.4, at 310 K. [HSA] = 1.00×10^{-6} M and [MTSC] = 1.32×10^{-5} M

residue can be found. This binding site was previously ascribed to the main binding site for some thiosemicarbazone derivatives [27, 57].

Knowing from fluorescence quenching and competitive binding studies that MTSC binds in Sudlow's site I, where the Trp-214 residue can be found, now it is important to know which amino acid residues are capable of interacting with this potential drug inside the protein pocket. For this, molecular docking calculations were carried out, with Figure 8 depicting the best docking score pose for HSA:MTSC.

Molecular docking results suggest that MTSC can interact inside Sudlow's site I via hydrogen bonding and hydrophobic forces. The thiosemicarbazone group of the ligand interacts by hydrogen bonding with the amino acid residues Asp-450 and Ser-453, within a distance of 2.10 Å for both residues. The

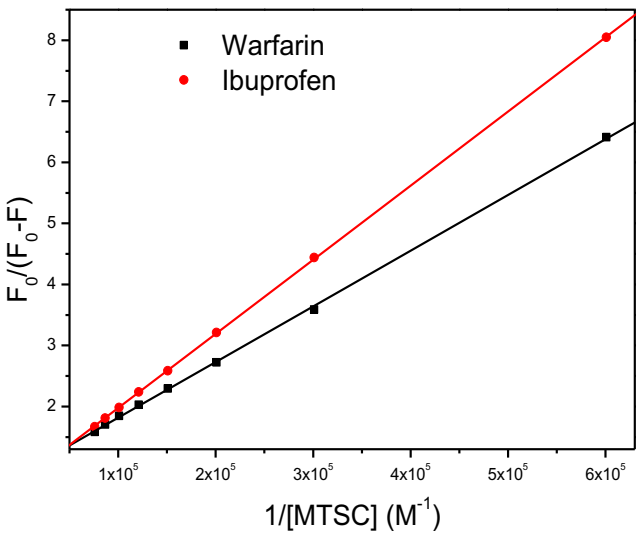

Fig. 7 Modified Stern-Volmer plots for interactions HSA:MTSC in the presence of site markers warfarin and ibuprofen, in PBS, at 310 K. [HSA] = 1.00×10^{-5} M, [MTSC] = 0.17, 0.33, 0.50, 0.66, 0.83, 0.99, 1.15, and 1.32×10^{-5} M

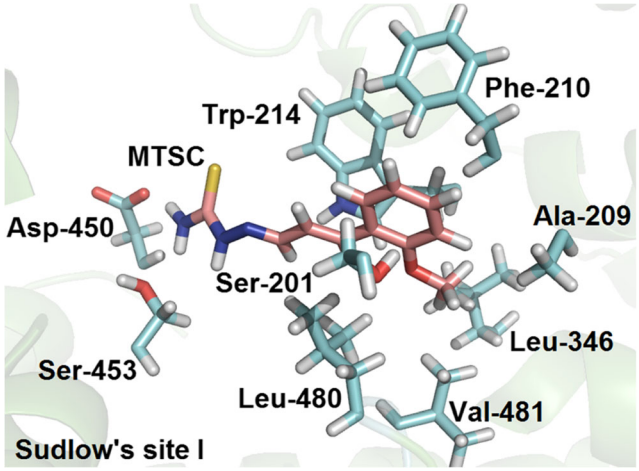

Fig. 8 Best docking pose for HSA:MTSC in Sudlow's site I, obtained by GOLD 5.2 program (*ChemPLP* function). Ligand structure is represented in beige, the green color is the HSA structure (PDB: 1N5U), the select amino acids residues are in cyan. Hydrogen: white; oxygen: red; nitrogen: dark blue and sulfur: yellow

oxygen of the methoxyl group in the aromatic ring of the ligand is a potential acceptor for hydrogen bonding with Ser-201 residue, within a distance of 3.80 Å. Furthermore, the hydrophobic moiety of the ligand is able to interact via hydrophobic forces with the amino acid residues Ala-209, Phe-210, Trp-214, Leu-346, Leu-480, and Val-481. In summary, molecular docking indicates that the intermolecular forces acting on the HSA:MTSC interaction are in agreement with those pointed out from the thermodynamic parameters obtained above ($\Delta H°$ and $\Delta S°$).

Conclusions

Cancer is the second leading cause of death in the world and until 2030 this group of diseases will be responsible for 17 million deaths (WHO). Furthermore, aging is directly associated with cancer incidence. The treatment can represent an obstacle in cancer therapy. The discovery of novel compounds that cure or prolong the patient's life considerably with the quality of life is necessary to change the future. Our data demonstrated that the novel thiosemicarbazone compound MTSC has cytotoxic activity *in vivo*. The chemotherapy-related toxicity is an important problem in patients' cancer treatment. Several reports of adverse anticancer drug reactions have been described, of which 50% were potentially fatal [58]. The treatment with MTSC did not induce any toxicity *in vivo*, suggesting that this compound did not cause adverse reactions and it is safe for mice. Failure of new anticancer drugs is related to poor absorption and bioavailability. Tumor cells take up albumin as a source of nitrogen and energy. To improve its cytotoxic effects,

some drugs, such as Paclitaxel and 5-Fluorouracil [59, 60], have been employed coupled with HSA. In our results, we observed that MTSC binds to HSA, suggesting that the effects observed *in vivo* depend on this interaction. These findings corroborated the higher capacity of this class of compounds to induce tumor cells' death. Fluorescence quenching studies showed that the interaction HSA:MTSC occurs *via* a ground-state association. Thermodynamic parameters indicate that this binding is moderate, spontaneous ($\Delta G^{\circ} < 0$), entropically, and enthalpically driven. Circular dichroism and synchronous fluorescence results suggest that the binding HSA:MTSC does not perturb significantly the secondary structure of the protein; however, it can change the microenvironment around the Trp-214 residue. Competitive binding studies in the presence of warfarin and ibuprofen show that the main binding site in HSA is Sudlow's site I. Finally, molecular docking results suggest that the potential drug can interact with the amino acid residues Ser-201, Ala-209, Phe-210, Trp-214, Leu-346, Asp-450, Asp-453, Leu-480, and Val-481 *via* hydrogen bonding and hydrophobic forces. The interaction of MTSC and HSA could provide therapeutic benefits, improving its cytotoxic efficacy and tolerability.

Acknowledgments The authors gratefully acknowledge the financial support from the Brazilian agencies: *Coordenação de Aperfeiçoamento de Pessoal de Nível Superior* (CAPES), *Conselho Nacional de Desenvolvimento Científico, Tecnológico* (CNPq), *Fundação de Amparo à Pesquisa do Estado do Rio de Janeiro* (FAPERJ) and *Programa de Oncobiologia* UFRJ. The authors acknowledge Profa. Dra. Nanci Camara de Lucas Garden (UFRJ) for the time-resolved and synchronous fluorescence facilities, as well as Prof. Dr. Carlos M.R. Sant'Anna (UFRRJ) for the computational facilities. O.A.C. acknowledges *Instituto Euvaldo Lodi* (IEL-Brazil) for the researcher grant in the SENAI Innovation Institute for Green Chemistry (Encomenda Rhae Trainee II - 404988/2017-2 -Process: 350173/2018-4). J.C.N.-F. acknowledges INMETRO for a Visiting Professor fellowship. The authors thank Dra. Vivian M. Rumjanek from *Instituto de Bioquímica Médica* of UFRJ for providing cell lines.

Funding The study was supported by Brazilian agencies: *Coordenação de Aperfeiçoamento de Pessoal de Nível Superior* (CAPES), *Conselho Nacional de Desenvolvimento Científico e Tecnológico* (CNPq) and *Fundação de Amparo à Pesquisa do Estado do Rio de Janeiro* (FAPERJ).

Compliance with ethical standards

Conflict of interest The authors declare that they have no conflict of interest.

Ethical approval The *in vivo* assays procedures were performed in accordance to the Brazilian Guidelines (Brazilian Directive for Care and Use of Animals for Teaching and Research-DBCA) published by the Brazilian Council for Control of Animal Experimentation (*Conselho Nacional de Controle de Experimentação Animal* – CONCEA) and Brazilian Federal Law 11.794 (October 8, 2008). The local research ethics committee of the *Universidade Federal Rural do Rio de Janeiro*, Brazil, approved the protocols used in the present study (Number 6985210617).

References

1. Beraldo H (2004) Semicarbazones and thiosemicarbazones: their wide pharmacological profile and clinical applications. Quim Nova 3:461–471
2. Smee DF, Sidwell RW (2003) A review of compounds exhibiting antorthopoxvirus activity in animal models. Antivir Res 57:41–52
3. Paiva RO, Kneipp LF, Goulart CM, Albuquerque MA, Echevarria A (2014) Antifungal activities of thiosemicarbazones and semicarbazones against mycotoxigenic fungi. Ciên Agrotec 38: 531–537
4. Dobek AS, Klayman DL, Dickson ET Jr, Scovill JP, Tramont EC (1980) Inhibition of clinically significant bacterial organisms in vitro by 2-acetylpyridine thiosemicarbazones. Antimicrob Agents Chemother 18:27–36
5. Soares ROA, Echevarria A, Bellieny MSS, Pinho RT, de Leo RMM, Seguins WS, Machado GM, Canto-Cavalheiro MM, Leon LL (2011) Evaluation of thiosemicarbazones and semicarbazones as potential agents anti-Trypanosoma cruzi. Exp Parasitol 129:381–387
6. Melos JLR, Torres-Santos EC, Faiões VS, Del Cistia CN, Sant'Anna CMR, Rodrigues-Santos CE, Echevarria A (2015) Novel 3,4-methylenedioxyde-6-X-benzaldehyde-thiosemicarbazones: Synthesis and antileishmanial effects against Leishmania amazonenses. Eur J Med Chem 103:409–417
7. Santos JS, Melos JLR, Lima GS, Lyra JC, Guedes GP, Rodrigues-Santos CE, Echevarria A (2017) Synthesis, anti-*Trypanosoma cruzi* activity and quantitative structure relationships of some fluorinated thiosemicarbazones. J Fluorine Chem 195:31-36.
8. Kalinowski DS, Yu Y, Sharpe PC, Islam M, Liao YT, Lovejoy DB, Kumar N, Bernhardt PV, Richardson DR (2007) Design, synthesis, and characterization of novel iron chelators: structure–activity relationships of the 2-benzoylpyridine thiosemicarbazone series and their 3-nitrobenzoyl analogues as potent antitumor agents. J Med Chem 50:3716–3729
9. Serda M, Kalinowski DS, Rasko N, Potůčková E, Mrozek-Wilczkiewicz A, Musiol R, Malecki JG, Sajewicz M, Ratuszna A, Muchowicz A, Gola J, Šimůnek T, Richardson D, Polanski J (2014) Exploring the anti-cancer activity of novel thiosemicarbazones generated through the combination of retro-fragments: dissection of critical Structure-Activity Relationships. PLoS One 9:e110291
10. Santos TAR, Silva AC, Silva EB, Gomes PATM, Espindola JWP, Cardoso MVO, Moreira DRM, Leite ACL, Pereira VRA (2016) Antitumor and immunoregulatory activities of thiosemicarbazones and 1,3-thiazoles in Jurkat and HT-29 cells. Biomed Pharmacother 82:555–560
11. Kalinowski DS, Quach P, Richardson DR (2009) Thiosemicarbazones: the new wave in cancer treatment. Future Med Chem 6:1143–1151
12. Krishnan K, Prathiba K, Jayaprakash V, Basu A, Mishra N, Zhou B, Hu S, Yen Y (2008) Synthesis and ribonucleotide reductase inhibitory activity of thiosemicarbazones. Bioorg Med Chem Lett 18: 6248–6250
13. French FA, Blanz EJ Jr (1965) The carcinostatic activity of α-(N)-heterocyclic carboxaldehydethiosemicarbazones. I. Isoquinoline-1-carboxaldehyde thiosemicarbazones. Cancer Res 25:1454–1458
14. Sharma N, Pathak DP (2016) Combatting challenging aspects of cancer with thiosemicarbazones. Int J Pharm Pharm Sci 8:27–34
15. Guo Z-L, Richardson DR, Kalinowski DS, Kovacevic Z, Tan-Un KC, Chan GC-F (2016) The novel thiosemicarbazone, di-2-pyridil ketone 4-cyclohexyl-4-methyl-3-thiosemicarbazone (DpC),

inhibits neuroblastoma growth in vitro and in vivo via multiple mechanism. J Hematol Oncol 9:1–16
16. Elsherbiny NM, Al-Gayyar MMH (2016) Anti-tumor activity of arjunolic acid against Ehrlich ascites carcinoma cells in vivo and in vitro through blocking TGF-β type 1 receptor. Biomed Pharmacother 82:28–34
17. Xu L, Hu Y-X, Li J, Liu Y-F, Zhang L, Ai H-X, Liu H-S (2017) Probing the binding reaction of cytarabine to human serum albumin using multispectroscopic techniques with the aid of molecular docking. J Photochem Photobiol B 173:187–195
18. Dorraji MSS, Azar VP, Rasoulifard MH (2014) Interaction between deferiprone and human serum albumin: Multi-spectroscopic, electrochemical and molecular docking methods. Eur J Pharm Sci 64:9–17
19. Burmudžija A, Ratković Z, Muškinja J, Janković N, Ranković B, Kosanić M, Đorđević S (2016) Ferrocenyl based pyrazoline derivatives with vanillic core: synthesis and investigation of their biological properties. RSC Adv 6:91420–91430
20. Wardell M, Wang Z, Ho JX, Robert J, Ruker F, Ruble J, Carter DC (2002) The atomic structure of human methemalbumin at 1.9 Å. Biochem Biophys Res Commun 291:913–918
21. Chaves OA, Amorim APO, Castro LHE, Sant'Anna CMR, de Oliveira MCC, Cesarin-Sobrinho D, Netto-Ferreira JC, Ferreira ABB (2015) Fluorescence and docking studies of the interaction between human serum albumin and pheophytin. Molecules 20: 19526–19539
22. Janković N, Muškinja J, Ratković Z, Bugarčić Z, Ranković B, Kosanić M, Stefanović S (2016) Solvent-free synthesis of novel vanillidene derivatives of Meldrum's acid: biological evaluation, DNA and BSA binding study. RSC Adv 6:39452–39459
23. Sharma R, Choudhary S, Kishore N (2012) Insights into the binding of the drugs diclofenac sodium and cefotaxime sodium to serum albumin: Calorimetry and spectroscopy. Eur J Pharm Sci 46:435–445
24. Demoro B, de Almeida RF, Marques F, Matos CP, Otero L, Pessoa JC, Santos I, Rodríguez A, Moreno V, Lorenzo J, Gambino D, Tomaz AI (2013) Screening organometallic binuclear thiosemicarbazone ruthenium complexes as potential anti-tumour agents: cytotoxic activity and human serum albumin binding mechanism. Dalton Trans 21:7131–7146
25. Karthikeyan S, Bharanidharan G, Kesherwani M, Mani KA, Srinivasan N, Velmurugan D, Aruna P, Ganesan S (2016) Insights into the binding of thiosemicarbazone derivatives with human serum albumin: spectroscopy and molecular modeling studies. J Biomol Struct Dyn 34:1264–1281
26. Xu Z, Liu Y, Zhou S, Fu Y, Li C (2016) Analysis of the Interaction of Dp44mT with human serum albumin and calf thymus DNA using molecular docking and spectroscopic techniques. Int J Mol Sci 17:1042–1057
27. Chaves OA, de Oliveira CHCS, Ferreira RC, Pereira RP, de Melos JLR, Rodrigues-Santos CE, Echevarria A, Cesarin-Sobrinho D (2017) Investigation of interaction between human plasmatic albumin and potential fluorinated anti-trypanosomal drugs. J Fluor Chem 199:103–112
28. Mosmann T (1983) Rapid colorimetric assay for cellular growth and survival: application to proliferation and cytotoxicity assays. Immunol Methods 65:55–63
29. Chaves OA, Jesus CSH, Cruz PF, Sant'Anna CMR, Brito RMM, Serpa C (2016) Evaluation by fluorescence, STD-NMR, docking and semi-empirical calculations of the o-NBA photo-acid interaction with BSA. Spectrochim Acta A 169:175–181
30. Wahba MEK, El-Enany N, Belal F (2015) Application of the Stern–Volmer equation for studying the spectrofluorimetric quenching reaction of eosin with clindamycin hydrochloride in its pure form and pharmaceutical preparations. Anal Methods 7:10445–10451
31. Chaves OA, Cesarin-Sobrinho D, Sant'Anna CMR, de Carvalho MG, Suzart LR, Catunda-Junior FEA, Netto-Ferreira JC, Ferreira ABB (2017) Probing the interaction between 7-O-β-D-glucopyranosyl-6-(3-methylbut-2-enyl)-5,4-dihydroxyflavonol with bovine serum albumin (BSA). J Photochem Photobiol A 336:32–41
32. Lakowicz JR (2006) Principles of Fluorescence Spectroscopy, 3rd edn. Springer, New York
33. Chaves OA, Soares BA, Maciel MAM, Sant'Anna CMR, Netto-Ferreira JC, Cesarin-Sobrinho D, Ferreira ABB (2016) A study of the interaction between trans-dehydrocrotonin, a bioactive natural 19-norclerodane, and serum albumin. J Braz Chem Soc 27:1858–1865
34. Simoni JA, Chagas AP (2007) Ellingham and Van't Hoff diagrams: some considerations. Quim Nova 30:501–504
35. Chaves OA, Teixeira FSM, Guimarães HA, Braz-Filho R, Vieira IJC, Sant'Anna CMR, Netto-Ferreira JC, Cesarin-Sobrinho D, Ferreira ABB (2016) Studies of the interaction between BSA and a plumeran indole alkaloid isolated from the stem bark of aspidosperma cylindrocarpon (Apocynaceae). J Braz Chem Soc 28:1229–1236
36. Matei I, Hillebrand M (2010) Interaction of kaempferol with human serum albumin: A fluorescence and circular dichroism study. J Pharm Biomed Anal 51:768–773
37. Khana SN, Islama B, Yennamalli R, Sultana A, Subbarao N, Khan AU (2008) Interaction of mitoxantrone with human serum albumin: Spectroscopic and molecular modeling studies. Eur J Pharm Sci 35: 371–382
38. Da Silva AP, Martini MV, de Oliveira CM, Cunha S, de Carvalho JE, Ruiz AL, da Silva CC (2010) Antitumor activity of (-)-alpha-bisabolol-based thiosemicarbazones against human tumor cell lines. Eur J Med Chem 45:2987–2993
39. De Oliveira JF, da Silva AL, Vendramini-Costa DB, Amorim CAC, Campos JF, Ribeiro AG, de Moura RO, Neves JL, Ruiz ALTG, de Carvalho JE, de Lima MCA (2015) Synthesis of thiophene-thiosemicarbazone derivatives and evaluation of their in vitro and in vivo antitumor activities. Eur J Med Chem 104:148–156
40. Wei L, Easmon J, Nagi RK, Muegge BD, Meyer LA, Lewis JS (2006) 64Cu-azabicyclo[3.2.2]nonane thiosemicarbazone complexes: radiopharmaceuticals for PET of topoisomerase II expression in tumors. J Nucl Med 47:2034–2041
41. Palanimuthu D, Shinde SV, Somasundaram K, Samuelson AG (2013) In vitro and in vivo anticancer activity of copper bis(thiosemicarbazone) complexes. J Med Chem 56:722–734
42. Narwal M, Kumar D, Mukherjee TK, Bhattacharyya R, Banerjee D (2018) Molecular dynamics simulation as a tool for assessment of drug binding property of human serum albumin. Mol Biol Rep. https://doi.org/10.1007/s11033-018-4308-3
43. Matsumura Y, Maeda H (1986) A new concept for macromolecular therapeutics in cancer chemotherapy: mechanism of tumoritropic accumulation of proteins and the antitumor agent smancs. Cancer Res 46:6387–6392
44. Nair MS (2015) Spectroscopic study on the interaction of resveratrol and pterostilbene with human serum albumin. J Photochem Photobiol B 149:58–67
45. Chaves OA, de Barros LS, de Oliveira MCC, Sant'Anna CMR, Ferreira ABB, da Silva FA, Cesarin-Sobrinho D, Netto-Ferreira JC (2017) Biological interactions of fluorinated chalcones: Stimulation of tyrosinase activity and binding to bovine serum albumin. J Fluor Chem 199:30–38
46. Joksimović N, Baskić D, Popović S, Zarić M, Kosanić M, Ranković B, Stanojković T, Novaković SB, Davidović G, Bugarčić Z, Janković N (2016) Synthesis, characterization, biological activity, DNA and BSA binding study: novel copper(ii) complexes with 2-hydroxy-4-aryl-4-oxo-2-butenoate. Dalton Trans 45:15067–15077
47. Montalti M, Credi A, Prodi L, Gandolfi MT (2006) Handbook of Photochemistry. 3rd ed. CRC Press, Taylor & Francis, Boca Raton
48. Tang B, Huang Y, Ma X, Liao X, Wang Q, Xiong X, Li H (2016) Multispectroscopic and docking studies on the binding of chlorogenic acid isomers to human serum albumin: Effects of esteryl position on affinity. Food Chem 212:434–442

49. Sengupta P, Sardar PS, Roy P, Dasgupta S, Bose A (2018) Investigation on the interaction of Rutin with serum albumins: Insights from spectroscopic and molecular docking techniques. J Photochem Photobiol B 183:101–110
50. Chaves OA, Jesus CSH, Henriques ES, Brito RMM, Serpa C (2016) In situ ultra-fast heat deposition does not perturb the structure of serum albumin. Photochem Photobiol Sci 15:1524–1535
51. Shi J-H, Pan D-Q, Jiang M, Liu T-T, Wang Q (2016) Binding interaction of ramipril with bovine serum albumin (BSA): Insights from multi-spectroscopy and molecular docking methods. J Photochem Photobiol B 164:103–111
52. Wang L, Zhang G, Wang Y (2014) Binding properties of food colorant allura red with human serum albumin in vitro. Mol Biol Rep 41:3381–3391
53. Miller JN (1979) Recent advances in molecular luminescence analysis. Proc Anal Div Chem Soc 16:203–208
54. Sun Z, Xu H, Cao Y, Wang F, Mi W (2016) Elucidating the interaction of propofol and serum albumin by spectroscopic and docking methods. J Mol Liq 219:405–410
55. Shahabadi N, Fili SM (2014) Molecular modeling and multispectroscopic studies of the interaction of mesalamine with bovine serum albumin. Spectrochim Acta A 118:422–429
56. Sudlow G, Birkett DJ, Wade DN (1976) Further characterization of specific drug binding sites on human serum albumin. Mol Pharm 12:1052–1061
57. Yu W, Shi L, Hui G, Cui F (2013) Synthesis of biological active thiosemicarbazone and characterization of the interaction with human serum albumin. J Lumin 134:491–497
58. Tuccori M, Montagnani S, Capogrosso-Sansone A, Mantarro S, Antonioli L, Fornai M, Blandizzi C (2015) Adverse reactions to oncologic drugs: spontaneous reporting and signal detection. Expert Rev Clin Pharmacol 8:61–75
59. Stinchcombe TE (2007) Nanoparticle albumin-bound paclitaxel: a novel Cremphor-EL-free formulation of paclitaxel. Nanomedicine 2:415–423
60. Koziol MJ, Sievers TK, Smuda K, Xiong Y, Müller A, Wojcik F, Steffen A, Dathe M, Georgieva R, Bäumler H (2014) Kinetics and efficiency of a methyl-carboxylated 5-Fluorouracil-bovine serum albumin adduct for targeted delivery. Macromol Biosci 14:428–439